Applied Mathematics and Computation 202 (2008) 596–607

Contents lists available at ScienceDirect

Applied Mathematics and Computation

journal homepage: www.elsevier.com/locate/amc

# On Steepest-Descent-Kaczmarz methods for regularizing systems of nonlinear ill-posed equations

A. De Cezaro [a], M. Haltmeier [b,*], A. Leitão [c], O. Scherzer [b]

[a] IMPA, Estr. D. Castorina 110, 22460-320 Rio de Janeiro, Brazil
[b] Department of Mathematics, University of Innsbruck, Technikerstrasse 21a, A-6020 Innsbruck, Austria
[c] Department of Mathematics, Federal University of St. Catarina, P.O. Box 476, 88040-900 Florianópolis, Brazil

ARTICLE INFO

*Keywords:*
Nonlinear systems
Ill-posed equations
Regularization
Steepest-descent method
Kaczmarz method

ABSTRACT

We investigate modified steepest-descent methods coupled with a loping Kaczmarz strategy for obtaining stable solutions of nonlinear systems of ill-posed operator equations. We show that the proposed method is a convergent regularization method. Numerical tests are presented for a linear problem related to photoacoustic tomography and a nonlinear problem related to the testing of semiconductor devices.



## 1. Introduction

In this paper, we propose a new method for obtaining regularized approximations of systems of nonlinear ill-posed operator equations.

The *inverse problem* we are interested in consists of determining an unknown physical quantity $x \in X$ from the set of data $(y_0, \ldots, y_{N-1}) \in Y^N$, where $X$, $Y$ are Hilbert spaces and $N \geqslant 1$. In practical situations, we do not know the data exactly. Instead, we have only approximate measured data $y_i^\delta \in Y$ satisfying

$$\|y_i^\delta - y_i\| \leqslant \delta_i, \quad i = 0, \ldots, N-1 \tag{1}$$

with $\delta_i > 0$ (noise level). We use the notation $\delta := (\delta_0, \ldots, \delta_{N-1})$. The finite set of data above is obtained by indirect measurements of the parameter, and this process being described by the model,

$$\mathrm{F}_i(x) = y_i, \quad i = 0, \ldots, N-1, \tag{2}$$

where $\mathrm{F}_i : D_i \subset X \to Y$, and $D_i$ are the corresponding domains of definition.

Standard methods for the solution of system (2) are based in the use of *iterative-type* regularization methods [1,7,13,16,19] or *Tikhonov-type* regularization methods [7,23,30,32,33] after rewriting (2) as a single equation $\mathrm{F}(x) = y$, where

$$\mathrm{F} := (\mathrm{F}_0, \ldots, \mathrm{F}_{N-1}) : \bigcap_{i=0}^{N-1} D_i \to Y^N \tag{3}$$

* Corresponding author.
*E-mail addresses:* decezaro@impa.br (A. De Cezaro), markus.haltmeier@uibk.ac.at (M. Haltmeier), aleitao@mtm.ufsc.br (A. Leitão), otmar.scherzer@uibk.ac.at (O. Scherzer).

0096-3003/$ - see front matter © 2008 Elsevier Inc. All rights reserved.
doi:10.1016/j.amc.2008.03.010

and $y := (y_0, \ldots, y_{N-1})$. However, these methods become inefficient if $N$ is large or the evaluations of $F_i(x)$ and $F_i'(x)^*$ are expensive. In such a situation, Kaczmarz-type methods [6,15,22,26], which cyclically consider each equation in (2) separately, are much faster [24] and are often the method of choice in practice.

For recent analysis of Kaczmarz-type methods for systems of ill-posed equations, we refer the reader to [4,10,11,17].

The starting point of our approach is the steepest-descent method [7,29] for solving ill-posed problems. Motivated by the ideas in [10,11], we propose in this article a *loping Steepest-Descent-Kaczmarz method* (L-SDK method) for the solution of (2). This iterative method is defined by

$$x_{k+1}^{\delta} = x_k^{\delta} - \omega_k \alpha_k s_k, \tag{4}$$

where

$$s_k := F_{[k]}'(x_k^{\delta})^* (F_{[k]}(x_k^{\delta}) - y_{[k]}^{\delta}), \tag{5}$$

$$\omega_k := \begin{cases} 1, & \|F_{[k]}(x_k^{\delta}) - y_{[k]}^{\delta}\| \geqslant \tau \delta_{[k]}, \\ 0, & \text{otherwise}, \end{cases} \tag{6}$$

$$\alpha_k := \begin{cases} \Phi_{\text{rel}}(\|s_k\|^2 / \|F_{[k]}'(x_k^{\delta}) s_k\|^2), & \omega_k = 1, \\ \alpha_{\min}, & \omega_k = 0. \end{cases} \tag{7}$$

Here, $\alpha_{\min} > 0$, $\tau \in [2, \infty)$ are appropriate chosen numbers (see (13) and (14)), $[k] := (k \bmod N) \in \{0, \ldots, N-1\}$, and $x_0^{\delta} = x_0 \in X$ is an initial guess, possibly incorporating some *a priori* knowledge about the exact solution. The function $\Phi_{\text{rel}} : (0, \infty) \to (0, \infty)$ defines a sequence of relaxation parameters and is assumed to be continuous, monotonically increasing, bounded by a constant $\alpha_{\max}$, and to satisfy $\Phi(s) \leqslant s$ (see Fig. 1).

If $M$ is an upper bound for $\|F_{[k]}'(x)\|$, then $\|s_k\|^2 / \|F_{[k]}'(x_k^{\delta}) s_k\|^2 \geqslant 1/M^2$ (cf. Lemma 3.2). Hence, the relaxation function $\Phi_{\text{rel}}$ needs only be defined on $[1/M^2, \infty)$. In particular, if one chooses $\Phi_{\text{rel}}(s) = \alpha_{\min}$ being constant on that interval, then $\alpha_k = \alpha_{\min}$ and the L-SDK method reduces to the loping Landweber–Kaczmarz (L-LK) method considered in [10,11]. The convergence analysis of the L-LK method requires $\alpha_{\min} \leqslant 1/M^2$, whereas the adaptive choice of the relaxation parameters in the present paper allows $\alpha_k$ being much larger than $1/M^2$.

The L-SDK method consists in incorporating the Kaczmarz strategy (with the loping parameters $\omega_k$) in the steepest-descent method. This strategy is analog to the one introduced in [11] regarding the Landweber–Kaczmarz iteration. As usual in Kaczmarz-type algorithms, a group of $N$ subsequent steps (starting at some multiple $k$ of $N$) shall be called a *cycle*. The iteration should be terminated when, for the first time, all $x_k$ are equal within a cycle. That is, we stop the iteration at

$$k_*^{\delta} := \arg\min\{lN \in \mathbb{N} : x_{lN}^{\delta} = x_{lN+1}^{\delta} = \cdots = x_{lN+N-1}^{\delta}\}. \tag{8}$$

Notice that $k_*^{\delta}$ is the smallest multiple of $N$ such that

$$x_{k_*^{\delta}} = x_{k_*^{\delta}+1} = \cdots = x_{k_*^{\delta}+N-1}. \tag{9}$$

In the case of noise free data, $\delta_i = 0$ in (1), we choose $\omega_k \equiv 1$ and the iteration (4)–(7) reduces to the *Steepest-Descent-Kaczmarz* (SDK) method, which is closely related to the *Landweber–Kaczmarz* (LK) method considered in [17].

It is worth noticing that, for noisy data, the L-SDK method is fundamentally different from the SDK method: The bang-bang relaxation parameter $\omega_k$ effects that the iterates defined in (4) become stationary if *all components* of the residual vector $\|F_i(x_k^{\delta}) - y_i^{\delta}\|$ fall below a pre-specified threshold. This characteristic renders (4)–(7) a regularization method (see Section 3). Another consequence of using these relaxation parameters is the fact that, after a large number of iterations, $\omega_k$ will vanish for some $k$ within each iteration cycle. Therefore, the computational expensive evaluation of $F_{[k]}'(x_k)^*$ might be loped, making the L-SDK method in (4)–(7) a fast alternative to the LK method in [17]. Since in praxis the steepest-descent method performs

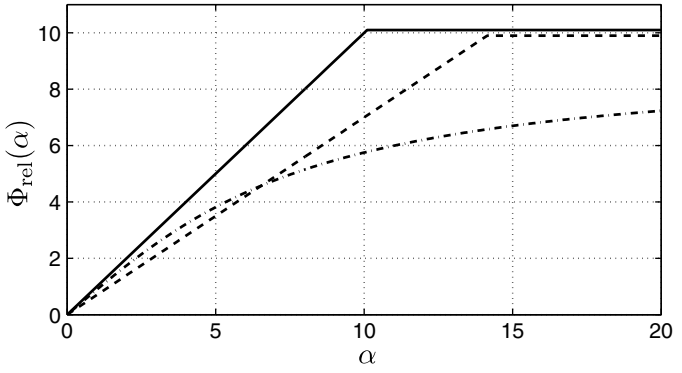


**Fig. 1.** Typical examples for relaxation function $\Phi_{\text{rel}}$.

better than the Landweber method, the L-SDK is expected to be more efficient than the L-LK method [10,11]. Our numerical experiments (mainly for the nonlinear problem considered in Section 5) corroborate this conjecture.

The article is outlined as follows. In Section 2, we formulate basic assumptions and derive some auxiliary estimates required for the analysis. In Section 3, we provide a convergence analysis for the L-SDK method. In Sections 4 and 5 we compare the numerical performance of the L-SDK method with other standard methods for inverse problems in photoacoustic tomography and in semiconductors, respectively.

## 2. Assumptions and basic results

We begin this section by introducing some assumptions, that are necessary for the convergence analysis presented in the following section. These assumptions derive from the classical assumptions used in the analysis of iterative regularization methods [7,16,29].

First, we assume that the operators $F_i$ are continuously Fréchet differentiable, and also assume that there exist $x_0 \in X$, $M > 0$, and $\rho > 0$ such that

$$\|F_i'(x)\| \leqslant M, \quad x \in B_\rho(x_0) \subset \bigcap_{i=0}^{N-1} D_i. \tag{10}$$

Notice that $x_0^\delta = x_0$ is used as starting value of the L-SDK iteration. Next we make an uniform assumption on the nonlinearity of the operators $F_i$.

Namely, we assume that the *local tangential cone condition* [7,16]

$$\|F_i(x) - F_i(\bar{x}) - F_i'(x)(x - \bar{x})\| \leqslant \eta \|F_i(x) - F_i(\bar{x})\|, \quad x, \bar{x} \in B_\rho(x_0) \tag{11}$$

holds for some $\eta < 1/2$. Moreover, we assume the existence of and element

$$x^* \in B_{\rho/2}(x_0) \text{ such that } F(x^*) = y, \tag{12}$$

where $y = (y_0, \ldots, y_{N-1})$ are the exact data satisfying (1).

We are now in position to choose the positive constants $\alpha_{\min}$, $\tau$ in (7) and (6). For the rest of this article, we shall assume

$$\alpha_{\min} := \Phi_{\text{rel}}(1/M^2), \tag{13}$$

$$\tau \geqslant 2\frac{1+\eta}{1-2\eta} \geqslant 2. \tag{14}$$

In particular, for linear problems we can choose $\tau$ equal to 2.

In the sequel we verify some basic results that are necessary for the convergence analysis derived in the next section. The first result concerns the well-definedness and positivity of the relaxation parameter $\alpha_k$.

**Lemma 2.1.** *Let assumptions (10)–(12) be satisfied. Then the coefficients $\alpha_k$ in (7) are well-defined and positive.*

**Proof.** If $\omega_k = 0$, the assertion follows from (7). If $\omega_k = 1$, then $\|F_{[k]}(x_k^\delta) - y_{[k]}^\delta\| \geqslant \tau\delta_{[k]}$ and the assertion is a consequence of [29, Lemma 3.1], applied to $F_{[k]}$ instead of F. □

In the next lemma, we prove an estimate for the step size of the L-SDK iteration.

**Lemma 2.2.** *Let $s_k$ and $\alpha_k$ be defined by (5) and (7). Then*

$$\alpha_k \|s_k\|^2 \leqslant \|F_{[k]}(x_k^\delta) - y_{[k]}^\delta\|^2, \quad k \in \mathbb{N}. \tag{15}$$

**Proof.** It is enough to consider the case $\omega_k = 1$. It follows from (7) that

$$\alpha_k \|s_k\|^2 = \Phi_{\text{rel}}\left(\frac{\|s_k\|^2}{\|F_{[k]}'(x_k^\delta)s_k\|^2}\right)\|s_k\|^2 \leqslant \frac{\|s_k\|^4}{\|F_{[k]}'(x_k^\delta)s_k\|^2}. \tag{16}$$

Moreover, from the definition of $s_k$ we obtain

$$\|F_{[k]}'(x_k^\delta)s_k\| = \|F_{[k]}'(x_k^\delta)F_{[k]}'(x_k^\delta)^*[F_{[k]}(x_k^\delta) - y_{[k]}^\delta]\|,$$
$$\|s_k\|^2 \leqslant \|F_{[k]}'(x_k^\delta)F_{[k]}'(x_k^\delta)^*[F_{[k]}(x_k^\delta) - y_{[k]}^\delta]\|\|F_{[k]}(x_k^\delta) - y_{[k]}^\delta\|.$$

Now, substituting the last two expressions in (16), shows (15). □

The following Lemma is an important auxiliary result, which will be used at several places throughout this article.

**Lemma 2.3.** *Let $x_k^\delta$, $\alpha_k$, $\omega_k$, and $s_k$ be defined by (4)–(7) and assume that (10)–(12) hold true. If $x_k^\delta \in B_{\rho/2}(x^*)$ for some $k \geqslant 0$, then*

$$\|x_{k+1}^\delta - x^*\|^2 - \|x_k^\delta - x^*\|^2 \leqslant \omega_k\alpha_k\|F_{[k]}(x_k^\delta) - y_{[k]}^\delta\|((2\eta - 1)\|F_{[k]}(x_k^\delta) - y_{[k]}^\delta\| + 2(1+\eta)\delta_{[k]}). \tag{17}$$

**Proof.** If $\omega_k = 0$, then $x_{k+1} = x_k$ and (17) follows with equality. If $\omega_k = 1$, it follows from (4) and (5) and Lemma 2.2 that

$$\begin{aligned}\|x_{k+1}^\delta - x^*\|^2 - \|x_k^\delta - x^*\|^2 &= 2\langle x_k^\delta - x^*, x_{k+1}^\delta - x_k^\delta\rangle + \|x_{k+1}^\delta - x_k^\delta\|^2 = 2\alpha_k\langle x_k^\delta - x^*, F'_{[k]}(x_k^\delta)^*(y_{[k]}^\delta - F_{[k]}(x_k^\delta))\rangle + \alpha_k^2\|s_k\|^2\\ &\leqslant 2k\alpha_k\langle y_{[k]}^\delta - F_{[k]}(x_k^\delta), F'_{[k]}(x_k^\delta)(x_k^\delta - x^*)\rangle + \alpha_k\|F_{[k]}(x_k^\delta) - y_{[k]}^\delta\|^2\\ &\leqslant \alpha_k(2\langle y_{[k]}^\delta - F_{[k]}(x_k^\delta), F'_{[k]}(x_k^\delta)(x_k^\delta - x^*) - F_{[k]}(x^*) + F_{[k]}(x_k^\delta)\rangle + 2\langle y_{[k]}^\delta - F_{[k]}(x_k^\delta), y_{[k]} - y_{[k]}^\delta\rangle\\ &\quad - \|y_{[k]}^\delta - F_{[k]}(x_k^\delta)\|^2).\end{aligned}$$

Now, applying (11) with $x = x^*$ and $\bar{x} = x_k^\delta \in B_{\rho/2}(x^*) \subset B_\rho(x_0)$, leads to

$$\|x_{k+1}^\delta - x^*\|^2 - \|x_k^\delta - x^*\|^2 \leqslant \omega_k\alpha_k\|F_{[k]}(x_k^\delta) - y_{[k]}^\delta\|(2\eta\|F_{[k]}(x_k^\delta) - y_{[k]}\| + 2\delta_{[k]} - \|F_{[k]}(x_k^\delta) - y_{[k]}^\delta\|).$$

The last inequality and (1) show (17). □

Our next goal is to prove a monotony property, known to be satisfied by other iterative regularization methods, e.g., by the Landweber [7], the steepest-descent [29], the LK [17], and the L-LK [11] method.

**Proposition 2.4** (Monotonicity). *Under the assumptions of Lemma 2.3,*

$$\|x_{k+1}^\delta - x^*\|^2 \leqslant \|x_k^\delta - x^*\|^2, \quad k \in \mathbb{N}. \tag{18}$$

*Moreover, all iterates $x_k^\delta$ remain in $B_{\rho/2}(x^*) \subset B_\rho(x_0)$ and satisfy (17).*

**Proof.** From (12) it follows that $x_0 \in B_{\rho/2}(x^*)$. If $\omega^\delta = 0$, then $x_1$ satisfies (18) with equality and $x_1 \in B_{\rho/2}(x^*) \subset B_\rho(x_0)$. If $\omega^\delta \neq 0$, then Lemma 2.3 implies

$$\|x_1^\delta - x^*\|^2 - \|x_0^\delta - x^*\|^2 \geqslant (2\eta - 1)\|F_0(x_0^\delta) - y^{\delta,0}\| + 2(1+\eta)\delta^0 \geqslant \delta_0((2\eta - 1)\tau + 2(1+\eta)) \geqslant 0.$$

Therefore (18), for $k = 0$, follows from (14). In particular, $x_1 \in B_{\rho/2}(x^*)$. An inductive argument implies (18) and that $x_k \in B_{\rho/2}(x^*) \subset B_\rho(x_0)$ for all $k \in \mathbb{N}$. The assertions therefore follows from Lemma 2.3. □

## 3. Convergence analysis of the loping Steepest-Descent-Kaczmarz method

In this section, we provide a complete convergence analysis for the L-SDK iteration, showing that it is a convergent regularization method in the sense of [7] (see Theorems 3.3 and 3.6 below). Throughout this section, we assume that (10)–(13) hold, and that $x_k^\delta$, $\alpha_k$, $\omega_k$, and $s_k$ are defined by Eqs. (4)–(7).

Our first goal is to prove convergence of the L-SDK iteration for $\delta = 0$. For exact data $y = (y_0, \ldots, y_{N-1})$, the iterates in (4) are denoted by $x_k$.[1]

**Lemma 3.1.** *There exists an $x_0$-minimal norm solution of (2) in $B_{\rho/2}(x_0)$, i.e., a solution $x^\dagger$ of (2) such that*

$$\|x^\dagger - x_0\| = \inf\{\|x - x_0\| : x \in B_{\rho/2}(x_0) \text{ and } F(x) = y\}.$$

*Moreover, $x^\dagger$ is the only solution of (2) in $B_{\rho/2}(x_0) \cap (x_0 + \ker(F'(x^\dagger))^\perp)$.*

**Proof.** Lemma 3.1 is a consequence of [13, Proposition 2.1]. A detailed proof can be found in [16]. □

**Lemma 3.2.** *For all $k \in \mathbb{N}$, we have $\alpha_k \geqslant \alpha_{\min}$.*

**Proof.** For $\omega_k = 0$ the claimed estimate holds with equality. If $\omega_k = 1$, it follows from (10) that

$$\|s_k\|^2/\|F'_{[k]}(x_k^\delta)s_k\|^2 \geqslant \|F'_{[k]}(x_k^\delta)\|^{-2} \geqslant 1/M^2.$$

Now the monotonicity of $\Phi_{\text{rel}}$ implies $\alpha_k \geqslant \Phi_{\text{rel}}(M^{-2}) = \alpha_{\min}$. □

Throughout the rest of this article, $x^\dagger$ denotes the $x_0$-minimal norm solution of (2). We define $e_k := x^\dagger - x_k$. From Proposition 2.4, it follows that (17) holds for all $k$. By summing over all $k$, this leads to

$$\sum_{i=0}^{\infty}\alpha_i\|y_{[i]} - F_{[i]}(x_i)\|^2 \leqslant \frac{\|x_0 - x^\dagger\|}{1 - 2\eta} < \infty. \tag{19}$$

Eq. (19) and the monotony of $\|e_k\|$ shown in Proposition 2.4 are main ingredients in the following proof of the convergence of the SDK iteration.

[1] This is a standard notation used in the literature.

**Theorem 3.3** (Convergence for exact data). *For exact data, the iteration $(x_k)$ converges to a solution of (2), as $k \to \infty$. Moreover, if*

$$\mathcal{N}(F'(x^\dagger)) \subseteq \mathcal{N}(F(x)) \quad \text{for all } x \in B_\rho(x_0), \tag{20}$$

*then $x_k \to x^\dagger$.*

**Proof.** From (18), it follows that $\|e_k\|$ decreases monotonically and therefore that $\|e_k\|$ converges to some $\epsilon \geqslant 0$. In the following, we show that $e_k$ is in fact a Cauchy sequence.

For $k = k_0 N + k_1$ and $l = l_0 N + l_1$ with $k \leqslant l$ and $k_1, l_1 \in \{0, \dots, N-1\}$, let $n_0 \in \{k_0, \dots, l_0\}$ be such that

$$\sum_{i_1=0}^{N-1} \|F_{i_1}(x_{Nn_0+i_1}) - y_{i_1}\| \leqslant \sum_{i_1=0}^{N-1} \|F_{i_1}(x_{Ni_0+i_1}) - y_{i_1}\|, \quad i_0 \in \{k_0, \dots, l_0\}. \tag{21}$$

Then, with $n := Nn_0 + N - 1$, we have

$$\|e_k - e_l\| \leqslant \|e_k - e_n\| + \|e_l - e_n\| \tag{22}$$

and

$$\begin{aligned} \|e_n - e_k\|^2 &= \|e_k\|^2 - \|e_n\|^2 + 2\langle e_n - e_k, e_n\rangle^2, \\ \|e_n - e_l\|^2 &= \|e_l\|^2 - \|e_n\|^2 + 2\langle e_n - e_l, e_n\rangle^2. \end{aligned} \tag{23}$$

For $k \to \infty$, the first two terms of (23) converge to $\epsilon - \epsilon = 0$. Therefore, in order to show that $e_k$ is a Cauchy sequence, it is sufficient to prove that $\langle e_n - e_k, e_n\rangle$ and $\langle e_n - e_l, e_n\rangle$ converge to zero as $k \to \infty$.

To that end, we write $i = Ni_0 + i_1$, $i_1 \in \{0, \dots, N-1\}$ and set $i^* := Nn_0 + i_1$. Then, using the definition of the Steepest-Descent-Kaczmarz iteration it follows that

$$\begin{aligned} |\langle e_n - e_k, e_n\rangle| &= \left|\sum_{i=k}^{n-1} \alpha_i \langle F'_{i_1}(x_i)^*(y_{i_1} - F_{i_1}(x_i)), x^\dagger - x_n\rangle\right| \leqslant \sum_{i=k}^{n-1} \alpha_i \left|\langle y_{i_1} - F_{i_1}(x_i), F'_{i_1}(x_i)(x^\dagger - x_{i^*}) + F'_{i_1}(x_i)(x_{i^*} - x_n)\rangle\right| \\ &\leqslant \sum_{i=k}^{n-1} \alpha_i \|y_{i_1} - F_{n_1}(x_i)\| \|F'_{i_1}(x_i)(x^\dagger - x_{i^*})\| + \sum_{i=k}^{l-1} \alpha_i \|y_{i_1} - F_{i_1}(x_i)\| \|F'_{i_1}(x_i)(x_{i^*} - x_n)\|. \end{aligned} \tag{24}$$

From (11), it follows immediately that

$$\|F'_{i_1}(x_i)(x^\dagger - x_{i^*})\| \leqslant (1+\eta)\|y_{i_1} - F_{i_1}(x_{i^*})\|. \tag{25}$$

Again using the definition of the Steepest-Descent-Kaczmarz iteration and Eqs. (7) and (10), it follows that

$$\|F'_{i_1}(x_i)(x_{i^*} - x_n)\| \leqslant M\|x_{i^*} - x_n\| \leqslant M \sum_{j=i_1}^{N-2} \alpha_j \|F'_j(x_{Nl_0+j})^*(F_j(x_{Nn_0+j}) - y_j)\| \leqslant \alpha_{\max} M^2 \sum_{j=0}^{N-1} \|F_j(x_{Nn_0+j}) - y_j\|. \tag{26}$$

Substituting (25) and (26) in (24) leads to

$$|\langle e_n - e_k, e_n\rangle| \leqslant c \sum_{i_0=k_0}^{n-1} \sum_{i_1=0}^{N-1} \alpha_i \|y_{i_1} - F_{i_1}(x_{Ni_0+i_1})\| \left(\sum_{j=0}^{N-1} \|F_j(x_{Nn_0+j}) - y_j\|\right) \leqslant c \sum_{i_0=k_0}^{n-1} \left(\sum_{i_1=0}^{N-1} \|y_{i_1} - F_{i_1}(x_{Ni_0+i_1})\|\right)^2$$

with $c := \alpha_{\max}(1 + \eta + \alpha_{\max} M^2)$. So, we finally obtain the estimate

$$|\langle e_n - e_k, e_n\rangle| \leqslant \frac{Nc}{\alpha_{\min}} \sum_{i_0=k_0}^{n-1} \sum_{i_1=0}^{N-1} \alpha_{Ni_0+i_1} \|y_{i_1} - F_{i_1}(x_{Ni_0+i_1})\|^2.$$

Because of (19), the last sum tends to zero for $k = Nk_0 + k_1 \to \infty$, and therefore $\langle e_n, e_n - e_k\rangle \to 0$. Analogously, one shows that $\langle e_n, e_n - e_l\rangle \to 0$. Therefore, $e_k$ is a Cauchy sequence and $x_k = x^\dagger - e_k$ converges to an element $x^* \in X$. Because all residuals $\|F_{[k]}(x_k) - y_{[k]}\|$ tend to zero, $x^*$ is solution of (2).

Now assume $\mathcal{N}(F'(x^\dagger)) \subseteq \mathcal{N}(F(x))$, for $x \in B_\rho(x_0)$. Then from the definition of $x_k$ it follows that

$$x_{k+1} - x_k \in \mathcal{R}(F'_{[k]}(x_k)^*) \subset \mathcal{N}(F'_{[k]}(x_k))^\perp \subset \mathcal{N}(F'(x_k))^\perp \subset \mathcal{N}(F'(x^\dagger))^\perp.$$

An inductive argument shows that all iterates $x_k$ are elements of $x_0 + \mathcal{N}(F'(x^\dagger))^\perp$. Together with the continuity of $F'(x^\dagger)$ this implies that $x^* \in x_0 + \mathcal{N}(F'(x^\dagger))^\perp$. By Lemma 3.1, $x^\dagger$ is the only solution of (2) in $B_{\rho/2}(x_0) \cap (x_0 + \mathcal{N}(F'(x^\dagger))^\perp)$, and so the second assertion follows. □

The second goal in this section is to prove that $x^{\delta}_{k^{\delta}_*}$ converges to a solution of (2), as $\delta \to 0$. First we verify that, for noisy data, the stopping index $k^{\delta}_*$ defined in (8) is finite.

**Proposition 3.4** (Stopping index). *Assume* $\delta_{\min} := \min\{\delta_0, \ldots, \delta_{N-1}\} > 0$. *Then* $k^{\delta}_*$ *defined in* (8) *is finite, and*

$$\|F_i(x^{\delta}_{k^{\delta}_*}) - y^{\delta}_i\| < \tau\delta_i, \quad i = 0, \ldots, N-1. \tag{27}$$

**Proof.** Assume that for every $l \in \mathbb{N}$, there exists $i(l) \in \{0, \ldots, N-1\}$ such that $x_{lN+i(l)} \neq x_{lN}$. From Proposition 2.4 follows that we can apply (17) recursively for $k = 1, \ldots, lN$ and obtain

$$-\|x_0 - x^*\|^2 \leqslant \sum_{k=1}^{lN} \omega_k \alpha_k \|F_{[k]}(x^{\delta}_k) - y^{\delta}_{[k]}\|(2(1+\eta)\delta_{[k]} - (1-2\eta)\|F_{[k]}(x^{\delta}_k) - y^{\delta}_{[k]}\|), \quad l \in \mathbb{N}.$$

Using the fact that either $\omega_k = 0$ or $\|F_{[k]}(x^{\delta}_k) - y^{\delta}_{[k]}\| \geqslant \tau\delta_{[k]}$, we obtain

$$\|x_0 - x^*\|^2 \geqslant (\tau(1-2\eta) - 2(1+\eta)) \sum_{k=1}^{lN} \omega_k \alpha_k \delta_{[k]} \|F_{[k]}(x^{\delta}_k) - y^{\delta}_{[k]}\|. \tag{28}$$

Eq. (28), Lemma 3.2 and the fact that $x_{l'N+i(l')} \neq x_{l'N}$ for all $l' \in \mathbb{N}$, imply

$$\|x_0 - x^*\|^2 \geqslant (\tau(1-2\eta) - 2(1+\eta)) l \alpha_{\min} \delta_{\min}(\tau\delta_{\min}), \quad l \in \mathbb{N}. \tag{29}$$

The right-hand side of (29) tends to infinity, which gives a contradiction. Consequently, $\{l \in \mathbb{N} : x_{lN+i} = x_{lN}, 0 \leqslant i \leqslant N-1\} \neq \emptyset$ and the infimum in (8) takes a finite value.

To prove (27), assume to the contrary, that $\|F_i(x^{\delta}_{k^{\delta}_*}) - y^{\delta}_i\| \geqslant \tau\delta_i$ for some $i \in \{0, \ldots, N-1\}$. From (6) and (8) it follows that, $\omega_{k^{\delta}_*} = 1$ and $x^{\delta}_{k^{\delta}_*+i} = x^{\delta}_{k^{\delta}_*+i+1}$, respectively. Thus, Proposition 2.4 and Lemma 2.1 imply

$$0 \leqslant (2\eta - 1)\|F_i(x^{\delta}_{k^{\delta}_*}) - y^{\delta}_i\| + 2(1+\eta)\delta_i < \delta_i((2\eta-1)\tau + 2(1+\eta)).$$

This contradicts (14), concluding the proof of (27). □

The last auxiliary result concerns the continuity of $x^{\delta}_k$ at $\delta = 0$. For $y, y^{\delta} \in Y^N$, $\delta > 0$, and $k \in \mathbb{N}$ we define

$$\Delta_k(\delta, y, y^{\delta}) := \omega_k F'_{[k]}(x^{\delta}_k)^*(F_{[k]}(x^{\delta}_k) - y^{\delta}_{[k]}) - F'_{[k]}(x_k)^*(F_{[k]}(x_k) - y_{[k]}).$$

**Lemma 3.5.** *For all* $k \in \mathbb{N}$,

$$\lim_{\delta \to 0} \sup\{\|\Delta_k(\delta, y, y^{\delta})\| : y^{\delta} \in Y^N, \|y_i - y^{\delta}_i\| \leqslant \delta_i\} = 0. \tag{30}$$

*Moreover,* $x^{\delta}_{k+1} \to x_{k+1}$, *as* $\delta \to 0$.

**Proof.** We prove Lemma 3.5 by induction. The case $k = 0$ is similar to the general case and is omitted.

Now, assume $k > 0$ and that (30) holds for all $k' < k$. First, we note that (30) and the continuity of $\Phi_{\text{rel}}$ obviously imply $x^{\delta}_{k+1} \to x_{k+1}$, as $\delta \to 0$. For the proof of (30) we consider two cases. In the first case, $\omega_k = 1$, we have

$$\|\Delta_k(\delta, y, y^{\delta})\| = \|F'_{[k]}(x^{\delta}_k)^*(F_{[k]}(x^{\delta}_k) - y^{\delta}_{[k]}) - F'_{[k]}(x_k)^*(F_{[k]}(x_k) - y_{[k]})\|.$$

In the second case, $\omega_k = 0$, we have $\|F_{[k]}(x^{\delta}_k) - y^{\delta}_{[k]}\| \leqslant \tau\delta^k$ and consequently

$$\begin{aligned}\|\Delta_k(\delta, y, y^{\delta})\| &\leqslant \|F'_{[k]}(x_k)^*(F_{[k]}(x_k) - y_{[k]})\| \leqslant \|F'_{[k]}(x^{\delta}_k)\|(\|F_{[k]}(x_k) - F_{[k]}(x^{\delta}_k)\| + \|F_{[k]}(x^{\delta}_k) - y^{\delta}_k\| + \|y^{\delta}_k - y_{[k]}\|) \\ &\leqslant \|F'_{[k]}(x^{\delta}_k)\|(\|F_{[k]}(x_k) - F_{[k]}(x^{\delta}_k)\| + (\tau+1)\delta_{[k]}).\end{aligned}$$

Now (30) follows from (10), the continuity of $F_{[k]}$ and $F'_{[k]}$, and the induction hypothesis (which implies $x^{\delta}_k \to x_k$). □

**Theorem 3.6** (Convergence for noisy data). *Assume* $(\delta^j_0, \ldots, \delta^j_{N-1})$ *is a sequence in* $(0, \infty)^N$ *with* $\lim_{j\to\infty} \delta^j_i = 0$. *Let* $(y^j_0, \ldots, y^j_{N-1})$ *be a sequence of noisy data satisfying*

$$\|y^j_i - y_i\| \leqslant \delta^j_i, \quad i = 0, \ldots, N-1, \quad j \in \mathbb{N}$$

*and let* $k^j := k_*(\delta^j, y^j)$ *denote the corresponding stopping index defined in* (8). *Then* $x^{\delta^j}_{k^j}$ *converges to a solution of* (2), *as* $j \to \infty$. *Moreover, if* (20) *holds, then* $x^{\delta^j}_{k^j} \to x^{\dagger}$.

**Proof.** Let $x^*$ denote the limit of the iterates $x_k$ which is a solution of (2), cf. Theorem 3.3. From Lemma 3.5 and the continuity of $F_i$ we know that, for any fixed $k \in \mathbb{N}$,

$$x^{\delta^j}_k \to x_k, \quad F_i(x^{\delta^j}_k) \to F_i(x_k), \quad \text{as } j \to \infty. \tag{31}$$

To show that $x_{k^j}^{\delta^j} \to x^*$, we first assume that $k^j$ has a finite accumulation point $k_*$. Without loss of generality we may assume that $k^j = k_*$ for all $j \in \mathbb{N}$. From Proposition 3.4 we know that $\|y_i^{\delta^j} - F_i(x_{k_*}^{\delta^j})\| < \tau\delta_i^j$ and, by taking the limit $j \to \infty$, that $y_i = F_i(x_{k_*})$. Consequently, $x_{k_*} = x^*$ and $x_{k_*}^j \to x^*$ as $j \to \infty$.

It remains to consider the case where $k^j \to \infty$ as $j \to \infty$. To that end let $\varepsilon > 0$. Without loss of generality we assume that $k^j$ is monotonically increasing. According to Theorem 3.3, we can choose $n \in \mathbb{N}$ such that $\|x_{k^n} - x^*\| < \varepsilon/2$. Eq. (31) implies that there exists $j_0 > n$ such that $\|x_{k^n}^{\delta^j} - x_{k^n}\| < \varepsilon/2$ for all $j \geqslant j_0$. This and Proposition 2.4 imply

$$\|x_{k^j}^{\delta^j} - x^*\| \leqslant \|x_{k^n}^{\delta^j} - x^*\| \leqslant \|x_{k^n}^{\delta^j} - x_{k^n}\| + \|x_{k^n} - x^*\| < \frac{\varepsilon}{2} + \frac{\varepsilon}{2} = \varepsilon, \quad \text{for } j \geqslant j_0.$$

Consequently, $x_{k^j}^{\delta^j} \to x^*$.

If (20) holds true, then by Theorem 3.3, $x^* = x^\dagger$. Therefore, $x_{k^j}^{\delta^j} \to x^\dagger$, which concludes the proof. □

**Remark 3.7.** In standard iterative regularization methods, the number of performed iterations plays the role of the regularization parameter [7,16]. A parameter choice rule corresponds to the choice of an appropriate stopping index $k_*^\delta = k(\delta, y^\delta)$.

For the loping Kaczmarz iterations analyzed in this article, the situation is quite different. If $k$ is fixed, then the iterates $x_k^\delta$, do *not* depend continuously on data $y_i^\delta$. However, for a fixed sequence $(\omega_k)$ of loping parameters, the iterates $x_k^\delta$ *do depend* continuously on $y_i^\delta$: now, the loping sequences $(\omega_k)$ play the role of the regularization parameters and the particular sequence $\omega_k = \omega_k(\delta, y^\delta)$, depending on $\delta_i$ and the noisy data $y_i^\delta$, is the a posteriori *parameter choice* rule.

## 4. Limited view problem in photoacoustic computed tomography

In this section, we compare the numerical performance of loping Kaczmarz methods applied to a system of linear equations related to a limited view problem in *photoacoustic computed tomography* [8,18,28,34].

Let $X := L^2(D)$ denote the Hilbert space of all square integrable functions in the unit disc $D \subset \mathbb{R}^2$, and let $Y$ denote the Hilbert space of all functions $y : [0,2] \to \mathbb{R}$ with $\|y\|^2 := \int_0^2 y(t)t\,dt < \infty$. We consider the system,

$$\mathbf{M}_i x = y_i, \quad i = 0, \ldots, N-1, \tag{32}$$

where $\mathbf{M}_i : X \to Y$,

$$(\mathbf{M}_i x)(t) := \frac{1}{\sqrt{\pi}} \int_{S^1} x(\xi_i + t\sigma)\, d\Omega(\sigma), \quad t \in [0,2], \tag{33}$$

correspond to a scaled version of the *circular mean Radon transform*. Solving (32) is the crucial step in three-dimensional photoacoustic computed tomography with integrating linear detectors [9,28], where the centers of integration, $\xi_i$, correspond to the positions of the linear detectors. We are particularly interested in the incomplete data case (limited view problem), where the centers $\xi_i = (\sin(\pi i/(N-1)), \cos(\pi i/(N-1)))$ are uniformly distributed on the semicircle $S_+^1 := \{\xi = (\xi^1, \xi^2) \in \partial D : \xi^1 \geqslant 0\}$. Micro-local analysis predicts, that if the centers do not cover the whole circle, certain details (the *invisible* boundaries) of $x$ outside the detection region (convex hull of $S_+^1$) cannot be recovered [21,27,35].

The operators $\mathbf{M}_i$ are linear, bounded, and satisfy $\|\mathbf{M}_i\| \leqslant 1$, [10]. For linear bounded operators, the *tangential cone condition* (11) is satisfied with $\eta = 0$. Consequently, the analysis of Section 3 applies, and the L-SDK method (4)–(7) provides a convergent regularization method for solving (32). The adjoint of $\mathbf{M}_i$, required in (5) is given by $(\mathbf{M}_i^* y)(\xi) = y(|\xi_i - \xi|)/\sqrt{\pi}$, [10].

In the following numerical examples, we consider the L-SDK method with either the choice $\Phi_{\text{rel}}(s) = \max(\alpha_{\min} s, 2)$ or $\Phi_{\text{rel}}(s) = \alpha_{\min}$ (which corresponds to the L-LK method). In both cases we use $\alpha_{\min} = 0.4$ or $\alpha_{\min} = 1$, and assume $N = 50$ measurements. The phantom $x^\dagger$, shown in the left picture of Fig. 2, consists of a superposition of characteristic functions and one Gaussian kernel. Data $y_i = \mathbf{M}_i x^\dagger$ were calculated via numerical integration with the trapezoidal rule and 4% noise was added, such that $\|y_i - y_i^\delta\|/\|y_i\| \approx 0.04$. In all examples $x_0 = 0$ was used as initial guess. The regularized solutions $x_{k_*^\delta}^\delta$ with $\alpha_{\min} = 0.4$ are depicted in Fig. 3. For both, the L-SDK L-LK method, all visible parts of the phantom $x^\dagger$ are reconstructed reliable.

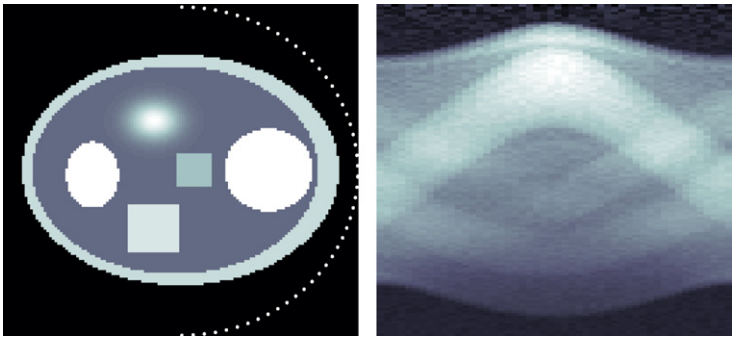

**Fig. 2.** The left picture shows the phantom $x^\dagger$, where the white dots indicate the locations of the detectors. The corresponding data $(y_i^\delta)_i$ are depicted on the right.

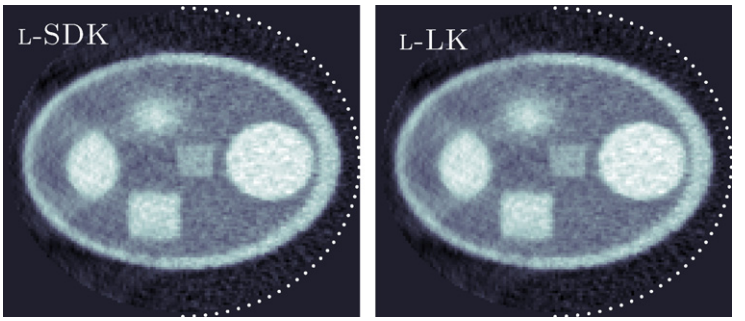


**Fig. 3.** Numerical reconstructions $x_{k_*^\delta}^\delta$ with $\alpha_{\min} = 0.4$ of the phantom depicted in Fig. 2.

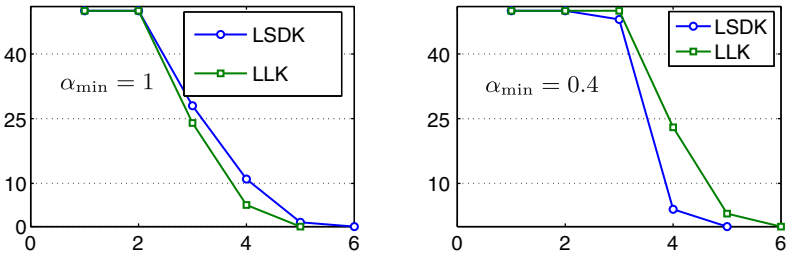


**Fig. 4.** The $x$-axis shows the number of cycles, while the number of actually performed iterations within each cycle is shown at the $y$-axis.

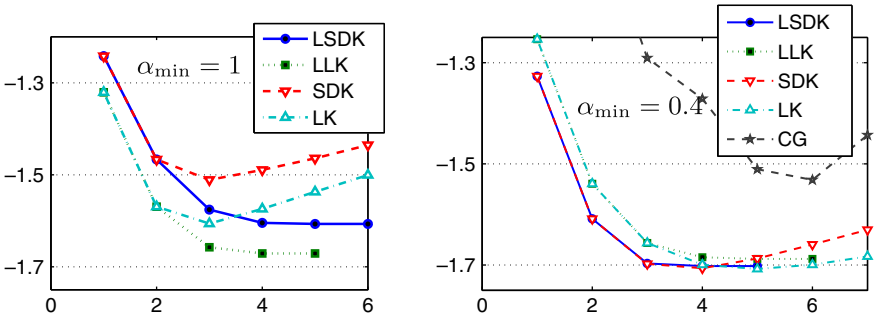


**Fig. 5.** Evolution of the relative error $\ln \|x^\dagger - x_k^\delta\| / \|x^\dagger\|$.

Figs. 4 and 5 show the number of actually performed iterations and the reconstruction error $e_k^\delta := \|x_k^\delta - x^\dagger\|$, respectively. For comparison purposes, the error for the SDK and the LK iteration (without loping parameter) are also included. In all cases, the smaller relaxation parameter $\alpha_{\min}$ gives the smaller reconstruction errors. This behavior is typically for the application of Kaczmarz-type iterations to Radon transforms [5,25]; therefore in praxis often relatively small relaxation parameters are chosen. For $\alpha_{\min} = 1$, the loping strategy significantly reduces the reconstruction error of the no-loping iterations. Also, for $\alpha_{\min} = 0.4$, the regularized solution of the loping Kaczmarz methods (automatically stopped according to (8)) have errors comparable to the optimal solution of their non-loping counterparts when stopped after the cycle with minimal error (which is not available in practice).

**Table 1**
Comparison of the performance of different iterative methods

| | Cycles | Runtime (s) | Error (%) |
|---|---|---|---|
| L-SDK | 5 | 21.9 | 18.2 |
| L-LK | 6 | 21.4 | 18.5 |
| SDK | 4 | 24.5 | 18.2 |
| LK | 5 | 16.9 | 18.1 |
| CGNE | 5 | 38.2 | 21.6 |

The non-loping iterations are stopped after the cycle with minimal error, whereas the loping Kaczmarz methods are automatically stopped according to (8).

To point out the effectiveness of the loping Kaczmarz methods for solving linear inconsistent systems we included the reconstruction error for the CGNE iteration (conjugate gradient [14,31] applied to normal equations). If stopped appropriately the CGNE method is known to be a regularization method [7,12]. As can be seen in Fig. 5 the reconstruction error for the L-SDK and the L-LK methods is much smaller that that for the CGNE iteration. In Table 1 run times for reconstructing an image on a $120 \times 120$ grid are compared (with non-optimized Matlab implementation on iMac with 2 GHz Intel Core Duo processor).

## 5. An inverse doping problem

In this section we present another comparison of the numerical performance of the L-SDK, L-LK and LK methods. This time we consider an application related to *inverse doping problems* for semiconductors [2,10,20,3]. For details on the mathematical modeling of this inverse problem we refer the reader to [10, Section 3].

In what follows, we describe the abstract formulation in Hilbert spaces of the problem (the so-called *inverse doping problem in the linearized unipolar model for current flow measurements*). Let $\Omega := (0,1) \times (0,1) \subset \mathbb{R}^2$ be the domain representing the semiconductor device (a diode). The two semiconductor contacts are represented by the boundary parts:

$$\Gamma_0 := \{(s,0) : \ s \in (0,1)\}, \quad \Gamma_1 := \{(s,1) : \ s \in (0,1)\},$$

(we denote $\partial\Omega_D := \Gamma_0 \cup \Gamma_1$) while the insulated surfaces of the semiconductor are represented by $\partial\Omega_N := \{(0,t) : t \in (0,1)\} \cup \{(1,t) : t \in (0,1)\}$. This specific inverse doping problem can be reduced to the identification of the positive parameter function $x$ (the doping profile $C$ is related to $x$ by $C = x - \lambda^2 \Delta(\ln x)$) in the model

$$\mu_n \nabla \cdot (x(\xi)\nabla u) = 0, \quad \text{in } \Omega \tag{34}$$

$$u = U(\xi), \quad \text{on } \partial\Omega_D \tag{35}$$

$$\nabla u \cdot \nu = 0, \quad \text{on } \partial\Omega_N \tag{36}$$

from measurements of the Voltage–Current map (the forward operator)

$$\Sigma_x : H^{3/2}(\partial\Omega_D) \to \mathbb{R},$$

$$U \mapsto \mu_n \int_{\Gamma_1} e^{V_{bi}(\xi)} u_\nu(\xi)\, d\Gamma,$$

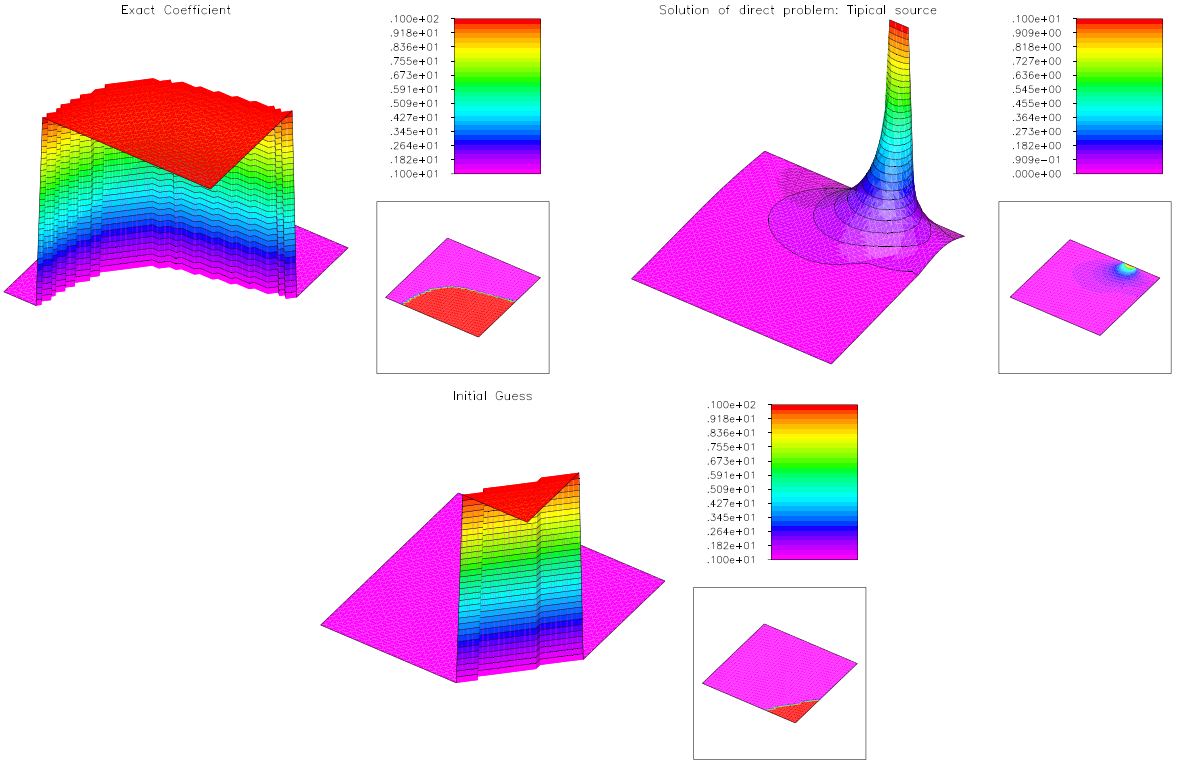


**Fig. 6.** In the top left picture, the doping profile to be identified. In the top right picture, a typical voltage profile $U_i$ and the corresponding solution $u$ of (34)–(36). The initial guess used for the L-SDK, L-LK and LK iterative methods is shown in the bottom picture. The boundary parts $\Gamma_0$ and $\Gamma_1$ correspond to the top right and to the lower left edge, respectively (the origin is the right corner).

which maps an applied potential $U$ at $\partial\Omega_D$ to the corresponding *total current flow* $\Sigma_x(U)$ through the contact $\Gamma_1$. Here $\mu_n$, $\lambda$ are positive constants and $V_{\mathrm{bi}}$ is a known logarithmic function defined on $\partial\Omega_D$.

Due to the nature of the practical experiments that can be performed on a factory environment, some restrictions on the data have to be taken into account:

1. The voltage profiles $U \in H^{3/2}(\partial\Omega_D)$ must satisfy $U(\xi) = 0$ at the contact $\Gamma_1$.
2. The parameter $x$ has to be determined from a finite number of measurements, i.e. from the data

$$y_i^\delta := \Sigma_x(U_i) \in Y := \mathbb{R}, \quad i = 0, \ldots, N-1, \tag{37}$$

where the $U_i \in H^{3/2}(\partial\Omega_D)$ are prescribed voltage profiles satisfying Item 1.

Therefore, we can model the inverse doping problem with a system of operator equations of the form (2), namely

$$F_i(x) = y_i^\delta, \quad i = 0, \ldots, N-1,$$

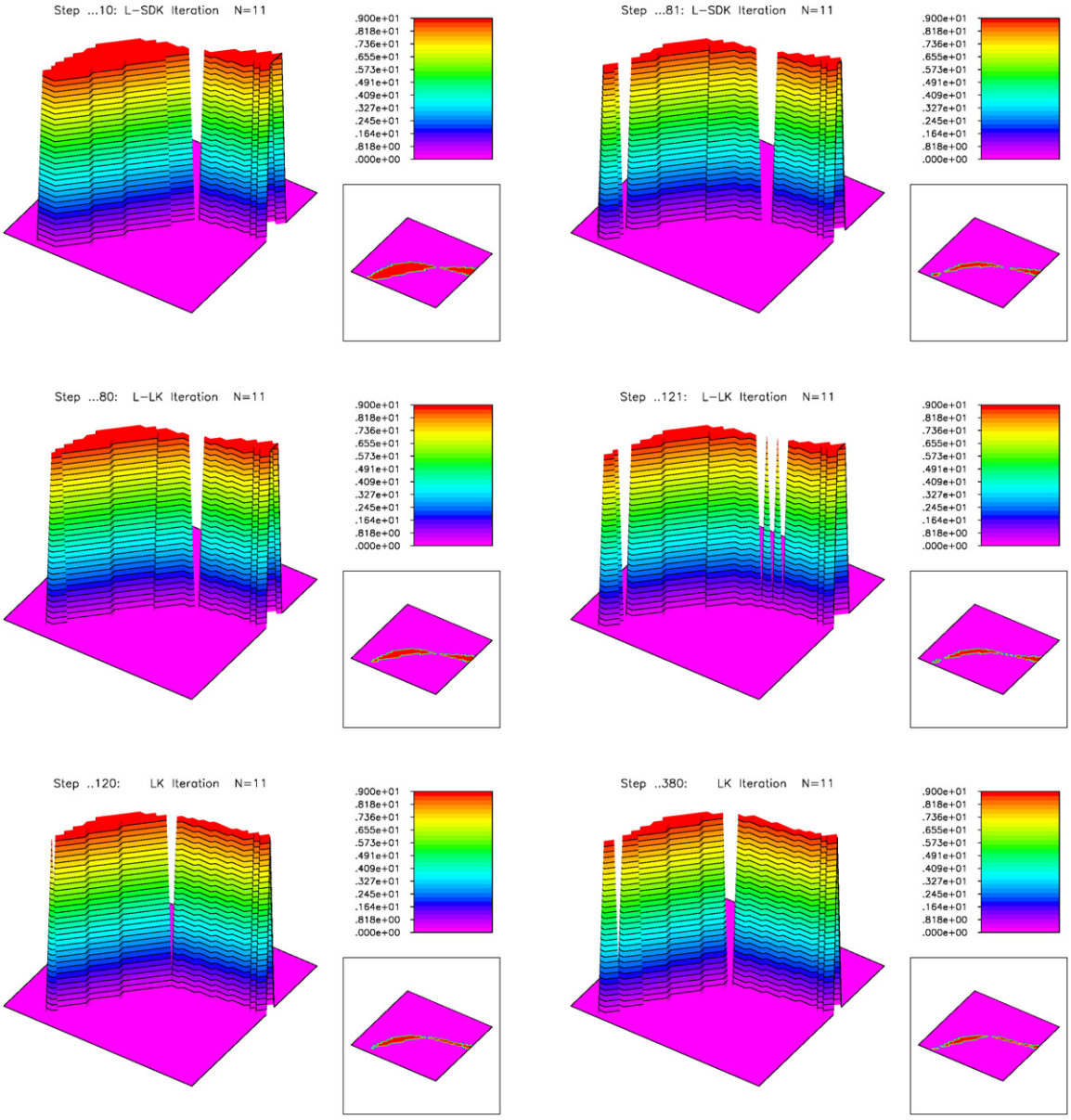


**Fig. 7.** Comparison between the L-SDK, L-LK and LK methods. The top two pictures show the iterative errors obtained by the L-SDK iteration after 10 and 81 cycles. The two central pictures show the iterative errors obtained by the L-LK iteration after 80 and 121 cycles. The two bottom pictures show the iterative errors obtained by the LK after 120 and 380 cycles.

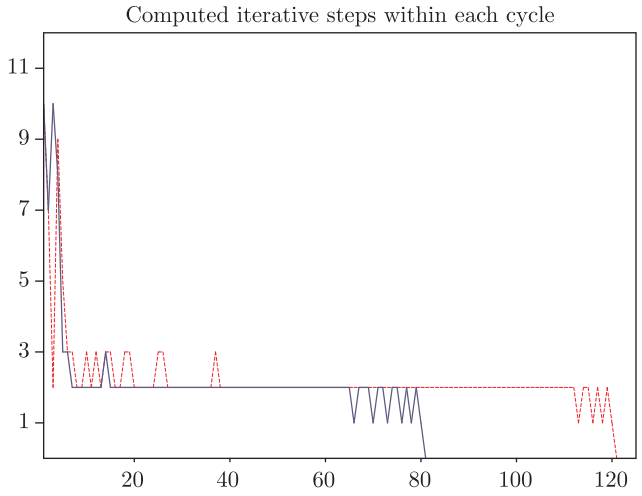


**Fig. 8.** Comparison between the performance of L-SDK and L-LK methods. The solid line shows the actually performed number of steps within each cycle of the L-SDK method, while the dashed line gives the corresponding information with respect to the L-LK method.

where $x \in L^2(\Omega) =: X$ is the unknown parameter, $y_i^\delta \in \mathbb{R} =: Y$ denote the measured data, $F_i : X \to Y$ defined by $F_i(x) := \Sigma_x(U_i)$ are the parameter to output maps, with domains of definition

$$D_i := \{x \in L^\infty(\Omega) : 0 < x_{\min} \leqslant x \leqslant x_{\max},\ \text{a.e.}\}.$$

It is worth mentioning that, although the operators $F_i$ are Fréchet differentiable, they do not satisfy the tangential cone condition (11). Therefore, the convergence results derived in Section 3 cannot be applied.

In the following numerical examples we assume that $N = 11$ Dirichlet–Neumann pairs $(U_i, F_i(x'))$ of measurement data are available. The fixed inputs $U_i$, are chosen to be piecewise constant functions supported in $\Gamma_0$,

$$U_i(s) := \begin{cases} 1, & |s - s_i| \leqslant h, \\ 0, & \text{else}, \end{cases}$$

where the points $s_i$ are uniformly distributed on $\Gamma_0$ and $h = 1/32$. The doping profile to be reconstructed is shown in Fig. 6 (top left picture). The top right picture of Fig. 6 shows a typical voltage profile $U_j$ (applied at $\Gamma_0$) as well as the corresponding solution $u$ of (34)–(36). In these pictures, as well as in the forthcoming ones, $\Gamma_1$ appears on the lower left edge and $\Gamma_0$ on the top right edge (the origin corresponds to the upper right corner).

In Fig. 7, we show the evolution of the iteration error for the L-SDK, L-LK and LK methods. The same initial guess was used for the three methods (see Fig. 6). In our computations we chose $\tau = 2.5$ in (14). The stopping rule for the L-SDK method is satisfied after 81 cycles. For the L-LK method, the same stopping criteria is reached only after 121 cycles. In order to obtain the same accuracy with the LK method, 380 cycles are required. In the top pictures of Fig. 7 one can see the iteration error for the L-SDK method after 10 and 81 cycles. For comparison purposes, the iteration error for the L-LK method is shown after 80 and 121 cycles (see the central pictures of Fig. 7). The bottom pictures of Fig. 7 show the iteration error for the LK method after 120 and 380 cycles. The number of actually computed iterative steps within each cycle of the L-SDK and L-LK methods is shown in Fig. 8.

As one can see in Fig. 8, no more than 2 steepest descent steps per cycle are computed after the 14th cycle of the L-SDK method. Analogously, no more than 2 Landweber steps per cycle are computed after the 37th cycle of the L-LK method. In total, for the computation of the LK-approximation in Fig. 7 (380 cycles), 4180 Landweber steps are needed, while the L-LK-approximation (121 cycles) requires the computation of 258 Landweber steps and the L-SDK-approximation (81 cycles) requires the computation of 184 steepest-descent steps. The L-LK method requires almost 50% more cycles than the L-SDK method in order to reach the stopping criteria (8). Moreover, the LK method requires almost three times more cycles than the L-LK method in order to achieve the same accuracy (see [10] for other comparisons between the LK and L-LK methods).

The efficiency of the L-SDK method becomes even more evident when we compare the total number of actually performed iterative steps. Each cycle of the LK method requires the computation of 11 steps, while in the L-SDK and L-LK methods the number of actually performed steps per cycle is very small after a few number of cycles.

## 6. Conclusions

In this paper, we propose a new iterative method for inverse problems of the form (2), namely the L-SDK method. As a by-product we also formulated the SDK iteration, which is the steepest-descent counterpart of the LK method [17]. In the L-SDK iteration, we omit an update of the SDK iteration (within one cycle) if corresponding $i$th residual is below some threshold.

Consequently, the L-SDK method is not stopped until all residuals are below the specified threshold. We provided a complete convergence analysis for the L-SDK iteration, proving that it is a convergent regularization method in the sense of Engl et al. [7].

The abstract theory was applied to thermoacoustic computed tomography and an inverse problem for semiconductors. In both applications the L-SDK method turned out to be an efficient iterative regularization method.

## Acknowledgements

The work of M.H. and O.S. is supported by the FWF (Austrian Science Fund) Grants Y-123INF and P18172-N02. The work of A.L. and A.DC. are supported by the Brazilian National Research Council CNPq, Grants 306020/2006-8 and 474593/2007-0. The authors thank Andreas Rieder for stimulating discussion on iterative regularization methods.

## References

[1] A.B. Bakushinsky, M.Y. Kokurin, Iterative methods for approximate solution of inverse problems, Mathematics and its Applications, vol. 577, Springer, Dordrecht, 2004.
[2] M. Burger, H.W. Engl, A. Leitão, P.A. Markowich, On inverse problems for semiconductor equations, Milan Journal of Mathematics 72 (2004) 273–313.
[3] M. Burger, H.W. Engl, P.A. Markowich, P. Pietra, Identification of doping profiles in semiconductor devices, Inverse Problems 17 (6) (2001) 1765–1795.
[4] M. Burger, B. Kaltenbacher, Regularizing Newton–Kaczmarz methods for nonlinear ill-posed problems, SIAM Journal on Numerical Analysis 44 (2006) 153–182.
[5] Y. Censor, P.P.B. Eggermont, D. Gordon, Strong underrelaxation in Kaczmarz's method for inconsistent systems, Numerische Mathematik 41 (1983) 83–92.
[6] P.P.B. Eggermont, G.T. Herman, A. Lent, Iterative algorithms for large partitioned linear systems, with applications to image reconstruction, Linear Algebra and Applications 40 (1981) 37–67.
[7] H.W. Engl, M. Hanke, A. Neubauer, Regularization of Inverse Problems, Kluwer Academic Publishers, Dordrecht, 1996.
[8] D. Finch, Rakesh, The spherical mean value operator with centers on a sphere, Inverse Problems 23 (6) (2007) S37–S49.
[9] P. Burgholzer, C. Hofer, G. Paltauf, M. Haltmeier, O. Scherzer, Thermoacoustic tomography with integrating area and line detectors, IEEE Transactions on Ultrasonics, Ferroelectrics, and Frequency Control 52 (2005) 1577–1583.
[10] M. Haltmeier, R. Kowar, A. Leitão, O. Scherzer, Kaczmarz methods for regularizing nonlinear ill-posed equations. II. Applications, Inverse Problems and Imaging 1 (3) (2007) 507–523.
[11] M. Haltmeier, A. Leitão, O. Scherzer, Kaczmarz methods for regularizing nonlinear ill-posed equations. I. Convergence analysis, Inverse Problems and Imaging 1 (2) (2007) 289–298.
[12] M. Hanke, Conjugate Gradient Type Methods for Ill-posed Problems, Longman Scientific & Technical, 1995.
[13] M. Hanke, A. Neubauer, O. Scherzer, A convergence analysis of Landweber iteration for nonlinear ill-posed problems, Numerische Mathematik 72 (1995) 21–37.
[14] M.R. Hestenes, E. Stiefel, On the convergence of the conjugate gradient method for singular linear operator equations, Journal of research of the National Bureau of Standards 49 (1952) 409–436.
[15] S. Kaczmarz, Approximate solution of systems of linear equations, International Journal of Control 57 (6) (1993) 1269–1271 (translated from German).
[16] B. Kaltenbacher, A. Neubauer, O. Scherzer, Iterative regularization methods for nonlinear ill-posed problems, de Gruyter, in press.
[17] R. Kowar, O. Scherzer, Convergence analysis of a Landweber–Kaczmarz method for solving nonlinear ill-posed problems, Ill Posed and Inverse Problems (Book Series) 23 (2002) 69–90.
[18] P. Kuchment, L.A. Kunyansky, Mathematics of thermoacoustic tomography, European Journal of Applied Mathematics 19 (2008) 191–224.
[19] L. Landweber, An iteration formula for Fredholm integral equations of the first kind, American Journal of Mathematics 73 (1951) 615–624.
[20] A. Leitao, P.A. Markowich, J.P. Zubelli, On inverse dopping profile problems for the stationary voltage–current map, Inverse Problems 22 (2006) 1071–1088.
[21] A.K. Louis, E.T. Quinto, Local Tomographic Methods in Sonar, Surveys on Solution Methods for Inverse Problems, Springer, Vienna, 2000. pp. 147–154.
[22] S. McCormick, The methods of Kaczmarz and row orthogonalization for solving linear equations and least squares problems in Hilbert space, Indiana University Mathematics Journal 26 (1977) 1137–1150.
[23] V.A. Morozov, Regularization Methods for Ill-posed Problems, CRC Press, Boca Raton, 1993.
[24] F. Natterer, Algorithms in tomography, State of the Art in Numerical Analysis 63 (1997) 503–524.
[25] F. Natterer, The Mathematics of Computerized Tomography, SIAM, Philadelphia, 2001.
[26] F. Natterer, F. Wübbeling, Mathematical Methods in Image Reconstruction, SIAM, Philadelphia, 2001.
[27] G. Paltauf, R. Nuster, M. Haltmeier, P. Burgholzer, Experimental evaluation of reconstruction algorithms for limited view photoacoustic tomography with line detectors, Inverse Problems 23 (6) (2007) S81–S94.
[28] G. Paltauf, R. Nuster, M. Haltmeier, P. Burgholzer, Photoacoustic tomography using a mach–zehnder interferometer as acoustic line detector, Applied Optics (2007) 3352–3358.
[29] O. Scherzer, A convergence analysis of a method of steepest descent and a two-step algorithm for nonlinear ill-posed problems, Numerical Functional Analysis and Optimization 17 (1–2) (1996) 197–214.
[30] T.I. Seidman, C.R. Vogel, Well posedness and convergence of some regularisation methods for non–linear ill posed problems, Inverse Problems 5 (1989) 227–238.
[31] J.R. Shewchuck, An introduction to the conjugate gradient method without the agonizing pain, Technical Report, School of Computer Science, Carnegie Mellon University, 1994.
[32] A.N. Tikhonov, Regularization of incorrectly posed problems, Soviet Mathematics Doklady 4 (1963) 1624–1627.
[33] A.N. Tikhonov, V.Y. Arsenin, Solutions of Ill-posed Problems (Fritz John, Trans.), John Wiley & Sons, Washington, DC, 1977.
[34] M. Xu, L.V. Wang, Photoacoustic imaging in biomedicine, Review of Scientific Instruments 77 (4) (2006) 041101.
[35] Y. Xu, L.V. Wang, G. Ambartsoumian, P. Kuchment, Reconstructions in limited-view thermoacoustic tomography, Medical Physics 31 (4) (2004) 724–733.